

Cite this article as: An Baijun, Li Yang, Li Jin, et al. Preparation of Water-based LFP/MXene Cathode for Lithium-Ion Battery by Inkjet Printing Method and Its Electrochemical Performance[J]. Rare Metal Materials and Engineering, 2022, 51(08): 2816-2821.

ARTICLE

# Preparation of Water-based LFP/MXene Cathode for Lithium-Ion Battery by Inkjet Printing Method and Its Electrochemical Performance

An Baijun, Li Yang, Li Jin, Shi Xingyu, Han Bo

Ningxia Key Laboratory for Photovoltaic Materials, Ningxia University, Yinchuan 750021, China

**Abstract:** LiFePO<sub>4</sub>(LFP)/Ti<sub>3</sub>AlC<sub>2</sub>(MXene) composites were prepared and then made into ink. Then LFP/MXene cathode was obtained by inkjet printing method. The effects of MXene content on the electrochemical performance of LFP were studied by adjusting the addition ratio of MXene to 2wt%, 3wt%, 4wt%, 5wt%, 6wt%. The results show that with the increase of MXene content, the electrochemical performance increases and then decreases. The optimal performance is obtained when the MXene addition ratio is 4wt%, at which the capacity increases to 181.2 mAh·g<sup>-1</sup>, and the Coulombic efficiency is 99.4% after 100 cycles. The reasons are that the MXene materials have an accordion layered structure so that the contact sites of lithium iron phosphate increases, and MXene materials have more functional group structure than graphene materials, which contributes to the electrochemical performance improvement of LFP. However, if excess MXene is added, agglomeration will occur which will affect its electrochemical performance.

**Key words:** LFP/MXene; electrochemical performance; inkjet printing

Li-ion batteries, which are applied to electricity grids, electric cars, variable renewable solar and wind generation etc, have attract increasing attention for their performance and cost improvements<sup>[1,2]</sup>. Among these Li-ion batteries materials, LiFePO<sub>4</sub> (LFP) is of great interests for its good safety, low cost, harmlessness, and environmental protection. Though it is widely used as cathode material for lithium-ion batteries, poor conductivity, low ion diffusion rate and small discharge ratio capacity restrict the further development of LFP<sup>[3-5]</sup>. In order to improve the performance of LFP, several methods and modifiers have been implemented<sup>[6-8]</sup>. 2D transition metal carbides/nitrides, Ti<sub>3</sub>AlC<sub>2</sub> (MXene), derived from MAX phase precursors, show potential for superior electrochemical performance, high energy density, and high power density for energy storage due to their remarkable electrical conductivity and low Li diffusion barrier<sup>[9-11]</sup>. Carbon-coated nanorod composites facilitate the charge transfer to enhance lithiation/delithiation kinetics, leading to an excellent rate performance and cycle stability<sup>[12]</sup>. However, carbon-coated LiMnPO<sub>4</sub> only delivers a lower specific capacity at corresponding current

densities<sup>[13]</sup>.

MXenes provide conductivity and alleviate the bulk expansion of active materials, while can provide high capacity and inhibit the selfstacking behavior<sup>[14]</sup>. Ti<sub>3</sub>C<sub>2</sub>T<sub>x</sub> is one of the most studied MXene materials<sup>[15]</sup>. The Ti<sub>3</sub>C<sub>2</sub>T<sub>x</sub> film prepared by spin steaming technology shows that the MXene sheets with abundant Li nucleation sites have a desirable affinity for Li<sup>[16]</sup>. Li et al<sup>[17]</sup> prepared LiFePO<sub>4</sub>/Ti<sub>3</sub>C<sub>2</sub> composite (LFP/TC) via a wet mixing method followed by a heat treatment. The LFP/TC composite with 2wt% Ti<sub>3</sub>C<sub>2</sub> (LFP/TC<sub>2</sub>) has the highest initial discharge capacity of 159 mAh·g<sup>-1</sup> at 0.1 C as well as the best rate performance with a reversible capacity of 86 mAh·g<sup>-1</sup> at 5 C. The Mn-doped LFP synthesized by a solvothermal process followed by a calcination at H<sub>2</sub>/Ar atmosphere offers rapid charge transfer channels with improved intercalation/de-intercalation kinetics of Li ions, which make as-synthesized LMFP@LiAlO<sub>2</sub>@C cathodes have outstanding rate capability and cycling stability<sup>[18]</sup>. Although much work has been done on the application of MXene materials to form LFP materials, the synthesis of

Received date: August 13, 2021

Foundation item: National Natural Science Foundation of China (51962030)

Corresponding author: Li Jin, Ph. D., Professor, Ningxia Key Laboratory for Photovoltaic Materials, Ningxia University, Yinchuan 750021, P. R. China, Tel: 0086-951-2077800, E-mail: lijn@nxu.edu.cn

Copyright © 2022, Northwest Institute for Nonferrous Metal Research. Published by Science Press. All rights reserved.

MXene and its composites of high performance by a facile method still faces great challenges<sup>[18-20]</sup>.

Inkjet printing is an important technology in printed electronics which has been used widely to develop conductive layers, interconnects, etc, on a variety of substrates<sup>[21,22]</sup>. Inkjet printing can directly deposit functional materials to form pattern onto substrate for flexible electronics as simple processes and printable complex patterns<sup>[23,24]</sup>. Yu et al<sup>[25]</sup> used the non-contact, mask-free digital inkjet printing to prepare the functional layers and electrodes of perovskite optoelectronic devices, providing a feasible and facile process route for the preparation of cathode ink for lithium-ion battery.

In the present work, the  $Ti_3AlC_2$  was prepared by high temperature melting method firstly, and then the  $Ti_3AlC_2$  was etched into two-dimensional layered MXene material by HF acid. The LFP/MXene composites were prepared by adding different proportions of two-dimensional layered MXene materials into LFP by mechanical dispersion and wet mixing. Furthermore, the composite material was prepared into printing ink and made into LFP/MXene cathode battery by inkjet printing, and the effect of addition amount on the electrochemical performance of LFP battery was investigated.

## 1 Experiment

### 1.1 Materials

Firstly,  $Ti_3C_2T_x$  was prepared and the process is shown in Fig. 1. TiC, Ti and Al powder were used as MAX precursor materials and dissolved in anhydrous ethanol in the required proportion. The reactant with anhydrous ethanol was poured into a beaker, placed in a water bath, and stirred at 70 °C for 2 h. Then the product was dried in a vacuum oven at 40 °C for 4 h. The dried product was taken out and put into the alumina crucible, and the crucible was put into the tubular furnace. In the atmosphere of high purity argon, it was heated to the set sintering temperature and kept for a period of time. After cooling to room temperature, the sample was taken out and ground into powder with agate mortar to obtain the precursor MXene. In a typical synthesis, 1.0 g MXene powder was poured into 10 mL HF solution and stirred at 40 °C for 40 h. The as-collected powders were washed clearly by deionized water for several times and then the product was dried in a vacuum drying oven at 70 °C.

A certain amount of commercial LFP particles were dissolved in ethanol. And then a certain amount of MXene powder prepared by the previous steps was dispersed in an appropriate amount of anhydrous ethanol for ultrasonic

dispersion for 30 min and magnetic stirring for 2 h. The dispersed MXene was poured into LFP dispersion solution for ultrasonic dispersion for 1 h, and the stirring was continued for 3 h under the condition of water bath at 40 °C. The MXene powder was blown and dried at 40 °C until the solvent was completely volatilized. The LFP/MXene composite was prepared by grinding the obtained material into powder in agate mortar. The composite was prepared into printing ink with solid content of 10%, and put into a bottle for use.

Lastly LFP/MXene composites were prepared by adding MXene materials with mass fractions of 2wt%, 3wt%, 4wt%, 5wt% and 6wt% , recorded as M2, M3, M4, M5 and M6, respectively. Then, the composites were prepared into ink and printed to prepare electrode. The button battery was printed by MP1100-type microelectronics printer.

### 1.2 Measurements

The morphology and structure of the LFP/MXene composites were characterized and analyzed by X-ray diffraction (XRD, DX-2700) with scan angle of 5°~90° and scanning electron microscope (F-SEM, JSM-7500F0). The button battery was tested on CHI660A electrochemical workstation to analyze its electrochemical performance. The Raman spectroscopy, contact angles and IR spectrum were tested by Thermo Scientific DXR, Dataphysics DCAT20, Spectrum Two, respectively.

## 2 Results and Discussion

### 2.1 Structural characterization

The XRD patterns of LFP/MXene composites are shown in Fig. 2a. According to PDF card #29-0095, (104) peak of the original  $Ti_3AlC_2$  phase at 39.1° is weakened obviously after HF etching, indicating that the Al atomic layer in  $Ti_3AlC_2$  crystal phase is removed<sup>[26]</sup>. Also, the (002) peak of M- $Ti_3C_2T_x$  appears at 8.5°. The corresponding layer spacing is about 1.04 nm. The peak of  $Ti_3AlC_2$  at 34° no longer appears, which indicates that the  $Ti_3AlC_2$  raw material is transformed into  $Ti_3C_2T_x$  after the Al atom layer is removed<sup>[27]</sup>. The infrared spectrum is shown in Fig. 2b, which indicates that the vibration absorption peaks of -PO group get the characteristic peak of LFP at 400~1500  $cm^{-1}$ . After adding MXene, the peak position does not shift and is in good agreement with that of pure lithium iron phosphate, which is consistent with the XRD pattern, indicating that no other impurities are generated during the synthesis of the composites. The infrared peaks at 2932, 2849 and 1725  $cm^{-1}$  correspond to the asymmetric stretching vibration peak of -CH, the asymmetric stretching vibration peak of -OH and the bending vibration peak of -OH, respectively, which are consistent with the infrared peak position of  $Ti_3C_2MXene$ , indicating that MXene exhibits excellent chemical stability in the process of synthesizing the composites<sup>[28]</sup>. The shift of hydroxy absorption band is usually related to the formation of hydrogen bond. The Raman spectra presented in Fig. 2c also support the conclusion. As shown in Fig. 2c, the Raman active vibration modes at 980 and 1035  $cm^{-1}$  are the out-of-plane vibration of A1g symmetry of Ti and

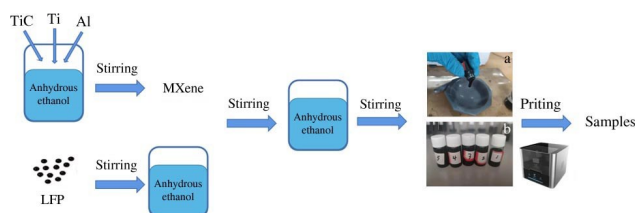


Fig.1 Schematic of synthesizing LFP/MXene

C atoms, respectively. While the vibration modes at 379, 446 and 581  $\text{cm}^{-1}$  are the plane vibration modes of Eg symmetry of Ti, C and surface functional group protons, respectively. Compared with the LFP material, the shift of the spectrum peak position is small<sup>[29]</sup>.

Fig. 2d presents the contact angle test results. It concludes that the contact angle of M4 is 32.2°, which is slightly larger than that of pure LFP ink, but smaller than that of graphene ink. This is due to the presence of O and F groups on the surface of MXene after hydrofluoric acid etching<sup>[30]</sup>. These O and F groups make MXene hydrophilic. However, the amount of MXene is not in a high level to improve the hydrophilicity of the ink much. In conclusion, the prepared LFP/MXene composites are structurally stable. There is no obvious impurity formation on account of the reasonable position and obvious peak intensity of each peak spectrum. The wettability of the prepared ink is improved, which is suitable for microelectronics printing.

## 2.2 Morphology characterization

Fig. 3 presents the typical SEM images of the samples at different magnifications. It shows that the MXene has compact 2D hierarchical structure. After HF etching, the precursor  $\text{Ti}_3\text{AlC}_2$  forms an accordion-like layered structure, which indicates that the Al layer is successfully etched.  $\text{Ti}_3\text{C}_2\text{T}_x$  is composed of stacked multiple lamellas, and there are obvious gaps between these lamellas, which is conducive to the binding of LFP particles<sup>[31]</sup>. Fig. 3a shows LFP electrode plates, which are used for comparison with MXene materials. Fig. 3b and 3c show the M2 and M3. The MXene composites on M2 and M3 are less distributed due to the small amount of MXene addition, and the size of MXene composites is also small. Moreover, the morphology of MXene composites is not

complete, and some parts are damaged. As a result, only a small amount of LFP combine with MXene<sup>[32]</sup>. Fig. 3e and 3f are the SEM images of sample M5 and M6. It shows that with the increase in MXene content in sample M5 and M6, the size of MXene composites is larger, and the layered structure becomes difficult to be observed. The distance between layers is reduced, and most of the layers are bonded together, which makes it difficult for LFP particles to be embedded in the layers, resulting in less binding between LFP and MXene. Fig. 3d shows the SEM image of M4. MXene composites of different sizes are distributed, and a large number of LFP particles are distributed on the surface of MXene and between the layers. We suppose that the addition of MXene can improve the dispersion performance of LFP particles, and the dispersion performance increases first and then decreases with the increase of MXene content. The addition amount of MXene also affects the size of MXene and the distance between layers, which is determined by both LFP content and MXene content.

## 2.3 Electrochemical analysis

To demonstrate the electrochemical performance of LFP/MXene composites, the composites were prepared into ink and printed to prepare electrode. Fig. 4a shows the first charge and discharge curves of LFP and LFP/MXene composites at 0.1 C between 2.5 and 4.2 V at room temperature. The charge and discharge curves are stable; the voltages are close to each other. With the increase of MXene content, the discharge capacity of the first cycle increases first and then decreases. The maximum first discharge specific capacity of sample M4 is 156.1  $\text{mAh}\cdot\text{g}^{-1}$ , and the first charge specific capacity is 157.5  $\text{mAh}\cdot\text{g}^{-1}$ , which is much higher than that of other samples. The discharge capacity is 91.8% of the theoretical capacity, while the discharge capacity of pure LFP is only 142

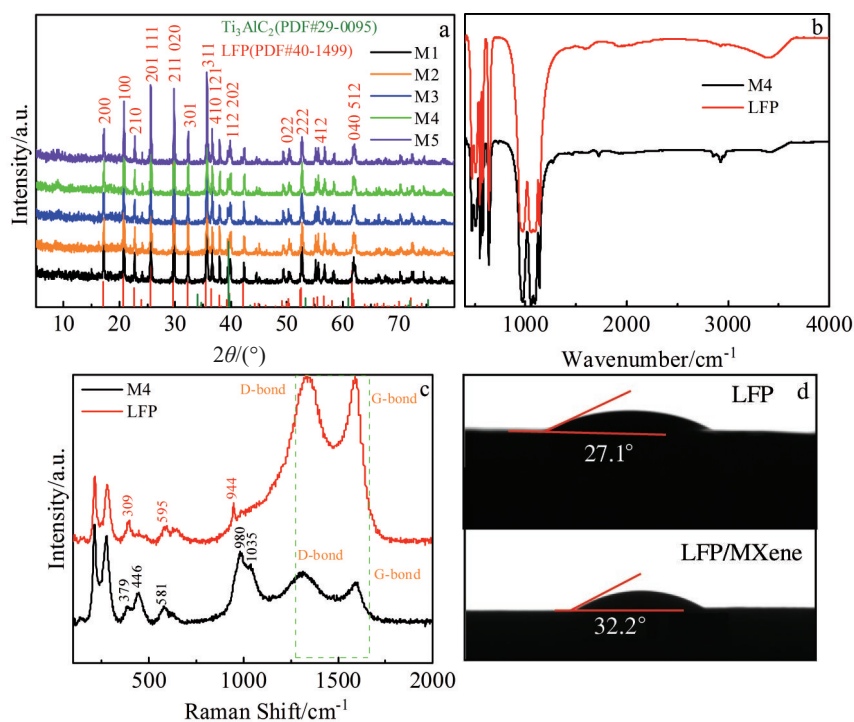


Fig. 2 XRD patterns (a), FTIR spectra (b), Raman spectra (c), and contact angle test diagram (d) of LFP/MXene composites

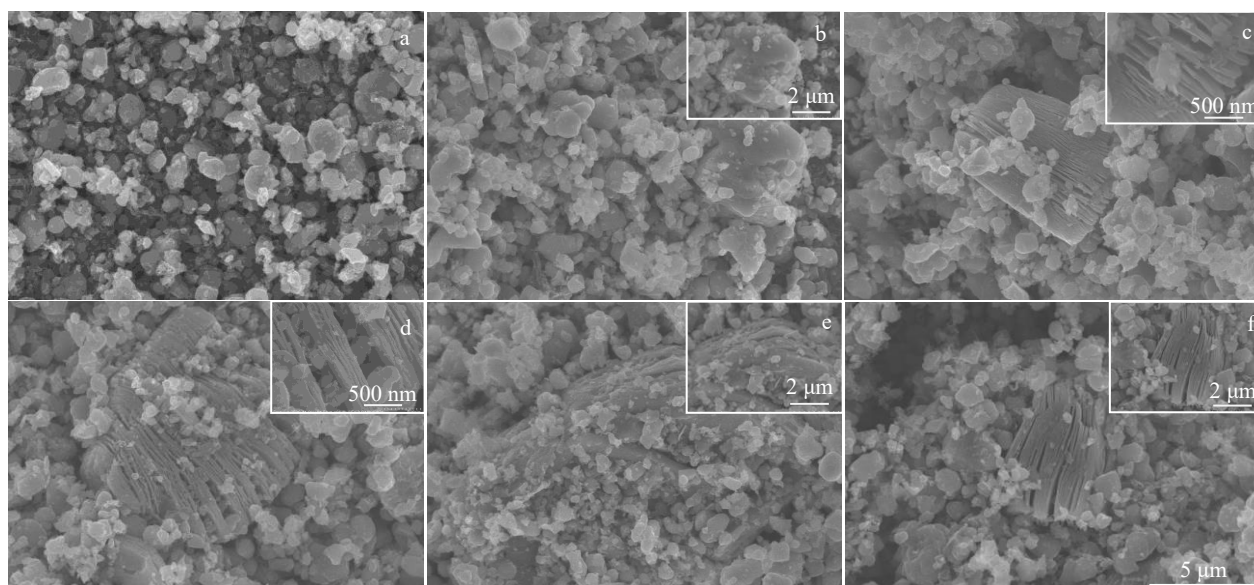


Fig.3 SEM images of LFP/MXene materials: (a) LFP, (b) M2, (c) M3, (d) M4, (e) M5, and (f) M6

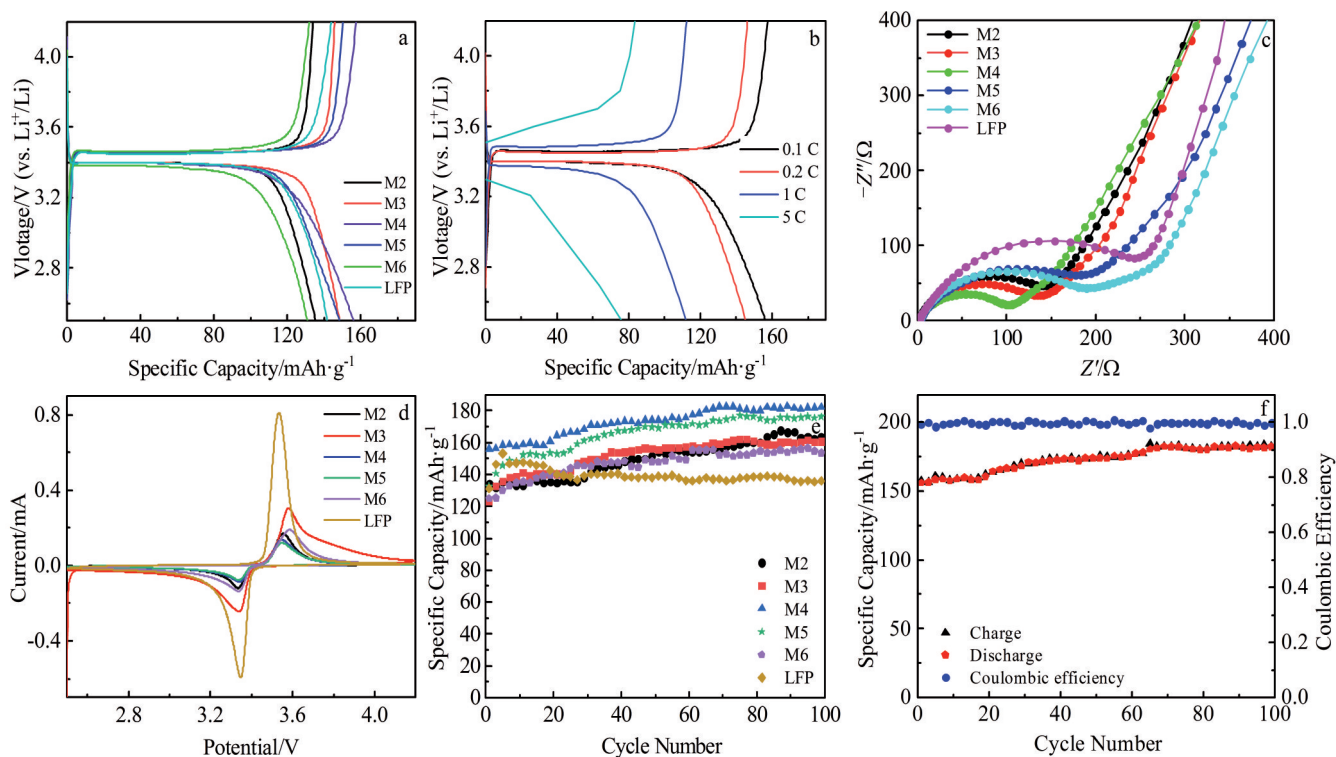


Fig.4 Electrochemical performance of LFP/MXene composites: (a, b) first charge-discharge curves, (c) EIS spectra, (d) C-V curves, (e) 100-cycle discharge capacity curves; (f) Coulombic cycle efficiency of sample M4

$\text{mAh}\cdot\text{g}^{-1}$  at 0.1 C. Furthermore, Fig.4b shows the charge and discharge tests of M4 at different rates. It is found that the charge and discharge capacity decrease sharply with the increase of the rate, indicating that the rate performance of the electrode is slightly improved after the addition of MXene. The reason is that the amount of MXene is less and the solid content of the prepared electrode ink is lower, but the charge and discharge capacity has been significantly improved at low rate<sup>[33]</sup>.

The semicircle size in the medium frequency region of the composites decreases after the addition of MXene, indicating that the charge transfers resistance ( $R_{ct}$ ) decreases, and the minimum  $R_{ct}$  of M4 is 101  $\Omega$ . With the increase of MXene content, the AC impedance first decreases and then increases because of conductivity of the electrode improved by adding MXene. Fig.4d shows the cyclic voltammetry curves of LFP and the composites at 0.1 mV/s sweep rate and in the 2.5~4.2 V voltage range. The oxidation peak and reduction peak of the

composites are gradually narrowed when the redox reaction occurs after the addition of MXene, indicating that there is no obvious polarization phenomenon in the charge-discharge process of the composites, which is more conducive to the electrode cycle.

The polarization phenomenon of sample M4 is the smallest, so as to the oxidation peak and the reduction peak<sup>[14,34]</sup>. With the addition of MXene, the cycling performance of LFP becomes better and the cycle number increases. The discharge specific capacity after 100 cycles is obviously improved, and the M4 shows the highest in cycling, reaching 181.2 mAh·g<sup>-1</sup>, and the Coulombic efficiency is 99.4% after 100 cycles, as shown in Fig. 4f. Li et al.<sup>[33]</sup> reported an ultrahigh reversible capacity of 1442 mAh·g<sup>-1</sup> at 0.1 A·g<sup>-1</sup> after 80 cycles. However, these composites usually have high initial irreversible capacity and low initial coulomb efficiency<sup>[35]</sup>. It is concluded from Fig. 4e that at 0.1 C for 100 cycles, the LFP/MXene shows higher discharge capacity than pure LFP. Due to the structural features, this novel structure prevents the stacking of MXene from providing a fast ion-diffusion path in phase (104). The accordion-like layered structures making the contact sites of lithium iron phosphate and MXene have more functional group structure than graphene. The transport properties and modification strategies of titanate-based compounds are benefited by enhancing the electronic conductivity and electrochemical performance. The MXene is more beneficial to improve the electrochemical performance of LFP electrode. The LFP particles dispersed over the MXene surfaces and layers accelerate the diffusion of lithium ions and the conduction of electrons, thus improving the electrochemical performance<sup>[36]</sup>.

### 3 Conclusions

1) The electrochemical performances of LFP are improved after adding MXene, which indicates that the addition of MXene as a two-dimensional layered conductive material can greatly improve the electronic conductivity of LFP, and further improve the electrochemical performances of the composite.

2) When MXene addition amount is 4wt%, the printing performance is the best. At this addition level, the LFP is embedded in the interlayer and surface, and has better combination and uniform dispersion.

3) The electrochemical performance of LFP/MXene electrode is improved compared with that of pure LFP electrode, and M4 has better first discharge capacity as high as 156.1 mAh·g<sup>-1</sup>. The voltage platform is the narrowest, and the AC impedance is 101 Ω. The maximum discharge capacity of M4 is 181.2 mAh·g<sup>-1</sup> after 100 cycles.

### References

- 1 Andre D, Kim S, Lamp P et al. *Journal of Materials Chemistry A* [J], 2015, 3: 6709
- 2 Crabtree G, Kocs E, Trahey L. *MRS Bull*[J], 2015, 40: 1067
- 3 Scrosati B, Garche J. *Journal of Power Sources*[J], 2010, 195:

- 2419
- 4 Bi Z Y, Zhang X D, He W et al. *RSC Advances*[J], 2013, 3: 19 744
- 5 Placke T, Kloepsch R, Duhnen S et al. *Journal of Solid State Electrochemistry*[J], 2017, 21: 1939
- 6 Nguyen V, Gu H B. *Journal of Applied Electrochemistry*[J], 2014, 44: 1153
- 7 Allah A E, Wang J, Kaneti Y V et al. *Nano Energy*[J], 2019, 65: 103 991
- 8 Li L, Zhang N, Zhang M Y et al. *Dalton Transactions*[J], 2019, 48: 1747
- 9 Naguib M, Kurtoglu M, Presser V et al. *Advanced Materials*[J], 2011, 23: 4248
- 10 Anasori B, Lukatskaya M R, Gogotsi Y. *Nature Reviews Materials*[J], 2017, 2: 17
- 11 Tang X, Guo X, Wu W J et al. *Advanced Energy Materials*[J], 2018, 8: 21
- 12 Chang H, Li Y, Fang Z K et al. *Applied Materials & Interfaces* [J], 2021, 13: 33 102
- 13 Yi T F, Peng P, Fang Z K et al. *Composites Part B: Engineering* [J], 2019, 175: 107 067
- 14 Ghidui M, Lukatskaya M R, Zhao M Q et al. *Nature*[J], 2014, 516: 78
- 15 Naguib M, Mochalin V N, Barsoum M et al. *Advanced Materials* [J], 2014, 26: 992
- 16 Wang C, Zheng Z, Feng Y et al. *Nano Energy*[J], 2020, 74: 104 817
- 17 Li X, Qian Y, Liu T et al. *Journal of Materials Science*[J], 2018, 53: 11 078
- 18 Yi T, Li Y, Fang Z et al. *Journal of Materiomics*[J], 2020, 6: 33
- 19 Wang Q, Peng D, Chen Y et al. *Journal of Electroanalytical Chemistry*[J], 2018, 818: 68
- 20 Song W, Liu J, You L et al. *Journal of Power Sources*[J], 2019, 419: 192
- 21 Gui N, Yang X, Tu J et al. *Powder Technology*[J], 2017, 318: 248
- 22 Yin Z P, Huang Y A, Bu N. *Chinese Science Bulletin*[J], 2010, 55: 3383
- 23 Salim A, Lim S. *Sensors*[J], 2017, 17: 20
- 24 Zhu D B, Wu M Q. *Journal of Electronic Materials*[J], 2018, 47: 5133
- 25 Yu C, Chen C, Wu D et al. *Chinese Journal of Liquid Crystals and Displays*[J], 2021, 36: 158 (in chinese)
- 26 Fell C, Chi M F, Meng Y S et al. *Solid State Ionics*[J], 2012, 207: 44
- 27 Lin Z, Rozier P, Duployer B et al. *Electrochemistry Communications*[J], 2016, 72: 50
- 28 Liu Y, Wang W, Ying Y L et al. *Dalton Transactions*[J], 2015, 44: 7123
- 29 Chien W, Li Y, Wu S et al. *Advanced Powder Technology*[J], 2020, 31(11): 4541
- 30 Luo J M, Tao X Y, Zhang J et al. *ACS Nano*[J], 2016, 10: 2491

- 31 Hemanth N R, Kandasubramanian B. *Chemical Engineering Journal*[J], 2020, 392: 123-678
- 32 Hu M M, Li Z J, Zhang H et al. *Chemical Communications*[J], 2015, 51: 13-531
- 33 Li M, Lu J, Luo K et al. *Journal of the American Chemical Society*[J], 2019, 141: 4730
- 34 Zhao M Q, Chang E, Ling Z et al. *Advanced Materials*[J], 2015, 27: 339
- 35 Jung B, Han C, Li B et al. *ACS Nano*[J], 2016(10): 2728
- 36 Yi T F, Wei T, Li Y et al. *Energy Storage Materials*[J], 2020, 26: 165

## 喷墨打印制备 LFP/MXene 阴极锂电池及其电化学性能

安百俊, 李 杨, 李 进, 石星宇, 韩 博  
(宁夏大学 宁夏光伏材料重点实验室, 宁夏 银川 750021)

**摘 要:** 制备了 MXene 含量 2%、3%、4%、5%、6% (质量分数) 的磷酸铁锂(LFP)/Ti<sub>3</sub>AlC<sub>2</sub>(MXene) 复合材料并将其制备成墨水, 通过喷墨打印方法得到锂离子阴极电池, 并研究了 MXene 含量对 LFP 电化学性能的影响。结果表明, 随着 MXene 含量的增加, LFP/MXene 复合材料的电化学性能先升高后降低。以 4%MXene 的添加剂制备得到的 LFP/MXene 复合材料电化学性能测试最佳, 其电容量达到 181.2 mAh·g<sup>-1</sup>, 100 次循环后其库仑效率为 99.4%。MXene 材料具有手风琴层状结构, 使得磷酸铁锂的接触比增加, 此外, MXene 材料比石墨烯材料具有更多的官能团结构, 有助于 LFP 的电化学性能改进。但如果 MXene 加入过多, MXene 材料发生结块, 会降低 LFP/MXene 复合材料电化学性能。

**关键词:** LFP/MXene; 电化学性能; 喷墨打印

---

作者简介: 安百俊, 男, 1987 年生, 博士生, 高级工程师, 宁夏大学 宁夏光伏材料重点实验室, 宁夏 银川 750021, 电话: 0951-2077800, E-mail: baianne@126.com